Journal of Renewable Materials

Tech Science Press

https://doi.org/10.32604/jrm.2026.02026-0063

ARTICLE

Experimental Investigation of Morphological, Physical, and Thermo-Mechanical Properties of Flax/Epoxy Composites for Automotive Applications

Matilde Oliveira[1], **Vítor Neves**[2] **and Mariana Banea**[1,*]

[1]CICECO—Aveiro Institute of Materials, Department of Materials and Ceramic Engineering, University of Aveiro, Aveiro, Portugal
[2]FTComposites, Lda., Rua Princesa Santa Joana N° 52, Quinta do Gato, Aveiro, Portugal

*Corresponding Author: Mariana Banea. Email: mbanea@ua.pt

Received: 03 May 2026; Accepted: 03 August 2026; Published: 23 September 2026

ABSTRACT: Natural fibre-reinforced composites are increasingly being considered as sustainable alternatives to synthetic composites for lightweight automotive applications. The aim of this study was to evaluate the influence of flax fibre architecture and areal weight on the mechanical, morphological, and thermal performance of epoxy-based composites. Laminates were manufactured by vacuum bagging using twill 2/2 and biaxial flax fabrics with areal weights of 200, 250, 350, and 400 g/m^2. Mechanical properties were assessed through tensile, flexural, and Charpy impact tests, while fracture mechanisms were analysed by scanning electron microscopy (SEM). Thermal behaviour was evaluated using thermogravimetric analysis (TGA) and differential scanning calorimetry (DSC). The results showed that fibre architecture and areal weight significantly affected composite performance. Twill 2/2 laminates exhibited the highest tensile (90.86 MPa) and flexural strengths (117.6 MPa). The highest impact strength was obtained for the biaxial fabric (LB) configuration (482 J/m). Composites reinforced with 200 g/m^2 fabrics showed the highest stiffness, with a Young's modulus of 8.31 GPa and a flexural modulus of 3.88 GPa. SEM analysis revealed good fibre-matrix adhesion and fibre pull-out as the dominant failure mechanisms. TGA indicated a two-stage degradation process, with major decomposition occurring between 300°C and 400°C and peak degradation temperatures between 340°C and 360°C. DSC analysis confirmed thermal stability typical of epoxy-based composites. Overall, the results demonstrate that flax fibre architecture and areal weight play a critical role in tailoring composite properties, highlighting their potential for sustainable lightweight automotive components.

KEYWORDS: Flax fibre; natural fibre composites; sustainability; automotive industry; fibre architecture; thermo-mechanical behaviour

1 Introduction

In recent years, natural fibre-reinforced composites have emerged as promising sustainable alternatives to conventional synthetic materials, particularly in the automotive sector. As this industry accounts for approximately 20% of global CO_2 emissions, there is increasing pressure to reduce its environmental footprint through the adoption of lightweight and eco-efficient materials. In this context, the development of bio-based composites represents a key strategy to decrease fuel consumption and associated emissions [1,2].

Among natural reinforcements, flax fibres have attracted considerable attention due to their competitive mechanical performance and environmental advantages when compared to traditional fibres such as glass, aramid (Kevlar), and carbon. These benefits include potential weight reductions of up to 30% and cost savings approaching 20% [3]. Furthermore, natural fibres offer additional advantages, including low density,

renewability, biodegradability, reduced energy consumption during production, and lower health and safety risks [4–7]. Specifically, flax fibres exhibit a favourable strength-to-weight ratio, along with good acoustic and thermal insulation properties, making them suitable for both structural and multifunctional applications across automotive, aerospace, and construction sectors [8–12].

Despite these advantages, natural fibres present inherent limitations that restrict their widespread structural application. These include moisture sensitivity, variability in fibre quality due to agricultural and extraction processes, limited thermal stability, and lower heat resistance compared to synthetic counterparts [13]. Addressing these challenges requires careful material design, particularly in terms of reinforcement architecture and processing conditions.

Natural fibre reinforcements are available in a wide range of textile architectures, including woven, braided, knitted, and non-woven mats, each imparting distinct mechanical behaviours to the resulting composites [14,15]. The selection of fabric architecture plays a critical role in determining key properties such as in-plane stiffness, interlaminar strength, and impact resistance. For example, Elayaraja and Rajamurugan [16] demonstrated that textile structure significantly influences damage tolerance and delamination behaviour, highlighting the importance of optimising reinforcement design for structural applications.

The mechanical performance of flax fibre-reinforced composites is strongly governed by both fibre architecture and fibre volume fraction. Several studies have investigated these effects. For example, Charlet et al. [17] demonstrated that the tensile properties of unidirectional flax fibre-reinforced composites are strongly governed by fibre orientation and fibre volume fraction. When fibres are highly aligned along the loading direction and present at sufficiently high volume fractions, these composites can achieve tensile strengths in the range of 100–130 MPa, with corresponding elastic moduli between 10–20 GPa. These values highlight the significant potential of flax fibres as structural reinforcements when optimal fibre alignment is ensured. In terms of flexural performance, Benkhelladi et al. [18] reported that the flexural strength of flax fibre-reinforced composites varies between 44.33 and 101.93 MPa, depending on fibre content and the application of chemical surface treatments. Their results indicate that fibre/matrix interfacial adhesion plays a critical role in bending performance, with treated fibres generally leading to improved stress transfer and enhanced mechanical properties. Similarly, Cerbu [19] observed pronounced anisotropy in flax/epoxy laminates, with tensile strengths reaching 70 MPa and flexural strengths up to 117 MPa, depending on fibre orientation.

In addition to mechanical performance, thermal behaviour is a critical consideration for automotive applications [20]. Dong et al. [21] investigated the thermal degradation of flax fibres and identified three stages in thermogravimetric analysis: initial moisture evaporation, primary degradation of hemicellulose and cellulose, and final char decomposition. The main degradation phase occurs between 340°C–370°C and is associated with the breakdown of hemicellulose and the cleavage of glycosidic bonds in cellulose, which defines the upper processing and service temperature limits of flax-based composites.

Although considerable progress has been made in the development and characterization of flax fibre-reinforced composites, the combined influence of textile architecture and fibre areal weight on the mechanical, morphological, and thermal performance of these materials remains insufficiently explored. Most previous studies have focused on individual parameters or specific loading conditions, resulting in a limited understanding of how fabric structure and reinforcement content interact to influence the overall behaviour of flax fibre composites, particularly for automotive applications.

Therefore, the objective of this study is to systematically investigate the effect of flax fabric architecture (twill 2/2 and biaxial) and fibre areal weight (200–400 g/m^2) on the physical, mechanical, morphological, and thermal properties of epoxy-based composites manufactured by vacuum bagging. Mechanical performance

was evaluated through tensile, flexural, and impact testing, while thermal behaviour was assessed using thermogravimetric analysis (TGA) and differential scanning calorimetry (DSC). In addition, scanning electron microscopy (SEM) was used to examine fracture surfaces and identify the dominant failure mechanisms.

2 Materials and Methods

Four different architectures of flax fabrics were used in this study: two twill fabrics with different grammages (L250 and L400) supplied from Emanuel Lang (Hirsingue, France), as well as a twill fabric (LT) and a biaxial fabric (LB) supplied by Bcomp (Fribourg, Switzerland). The fundamental properties of these fabrics, as provided by the manufacturers, are summarized in Table 1. The natural fibres remained untreated, with no surface modifications applied. A commercially available bi-component epoxy resin system, widely used in composite manufacturing, was selected as matrix resin. SR8100 epoxy resin was combined with SD8824 hardener in a 100:22 weight ratio, supplied by Sicomin Epoxy Systems (Châteauneuf-les-Martigues, France).

Table 1: Basic parameters of the fabrics and the composites produced.

Sample	Fabric Architecture	Areal Weight (g/m^2)	Fibre Density*	Fibre Thickness (mm)*	Fibre wt.%	Resin wt.%	Fibre Volume (%)
L250	Twill 2/2	250	1.30	0.40	35	65	32.51
L400		400	1.30	0.55	35	65	32.26
LT		200	1.35	0.50	30	70	28.54
LB	Biaxial	350	1.47	0.75	32	68	30.63

Note: *data from the technical datasheet.

2.1 Specimen Manufacturing

All flax composites with different reinforcement architectures were fabricated using vacuum-assisted resin infusion (VARI). The fabrics were first cut to 350 mm × 350 mm, and a mould-release wax was applied to the glass processing table. To remove moisture that could affect resin polymerization and weaken the composites, the flax fabrics were pre-dried at 60°C for 1 h under vacuum, as recommended by the supplier. After drying, the fibre mass of each sample was measured, and the composite lay-up was manually assembled (Fig. 1a).

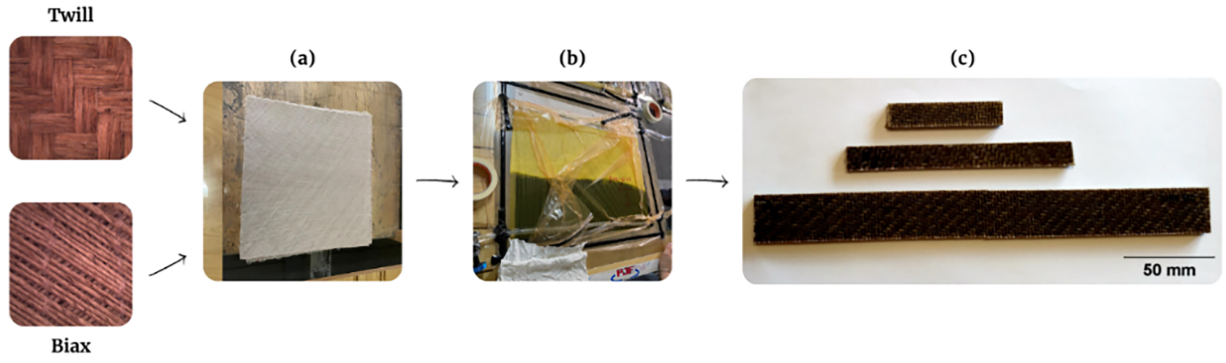

Figure 1: Composite specimen manufacturing process: (**a**) Lay-up of the fibres; (**b**) VARI processing; (**c**) Final composites with dimensions for mechanical testing.

The epoxy resin SR 8100 and hardener SD 8824 were mixed at a weight ratio of 100:22 (resin: hardener), according to the manufacturer's recommendations. The resin system was manually stirred for approximately

2 min until a homogeneous mixture was obtained. Resin infusion was then performed under a vacuum level of approximately −0.9 bar, while the infusion rate and vacuum tightness were carefully controlled to ensure complete fabric impregnation and minimise void formation. The process was continued until full wetting of the reinforcement was achieved (Fig. 1b).

After infusion, the laminates were cured at room temperature overnight and subsequently post-cured at 60°C for 3 h. Fig. 1 presents a schematic representation of the overall composite manufacturing process.

Finally, the plates were cut into specimens using water jet cutting, following the dimensions specified in the relevant ASTM standards: D3039/D3039M-14 for tensile tests (250 mm × 25 mm) [22] and D7264/D7264M-15 for flexural tests (125 mm × 13 mm) [23]. The impact test specimens (64 mm × 13 mm) were prepared based on the dimensions specified in ASTM D4812-11 [24]; however, the impact loading was performed in a simply supported Charpy configuration. Consequently, ASTM D4812 was used only as a reference for specimen dimensions, and the tests should be regarded as a modified Charpy impact method. A uniform thickness of approximately 4 mm was used to meet the minimum requirements for the mechanical tests. Accordingly, batch L250 consisted of 11 layers, L400 and LT of 8 layers, and LB of 6 layers.

2.2 Measurements and Characterization

2.2.1 Morphological Analysis

For fibre characterisation, scanning electron microscopy (SEM) was conducted using an Analytical UHR Schottky field emission microscope (SU-70, Hitachi, Tokyo, Japan), operated at an accelerating voltage of 8 kV. Fibre diameters were measured using ImageJ software (version 1.54d). For each fibre architecture, five individual measurements were performed, and the reported values correspond to the average of these measurements. Fractographic analysis was carried out on the LT batch, selected as a representative case to illustrate the failure behaviour of this class of materials after tensile testing. SEM analyses were carried out using a low-vacuum microscope (TM4000Plus, Hitachi, Tokyo, Japan) operated at an accelerating voltage of 10 kV. Prior to analysis, all samples were sputter-coated with a thin gold–palladium layer using a K950X Turbo Evaporator (Emitech, Montigny-le-Bretonneux, France) to enhance surface conductivity and prevent charging effects.

2.2.2 Density Characterization

Density was characterized using two distinct methods: the geometric method (Eq. (1)) and the Archimedes method (Eq. (2)).

$$\rho = \frac{m}{V} \tag{1}$$

$$\rho_{apparent} = \frac{M_D}{M_W - M_I} \times \rho_{liquid} \tag{2}$$

where ρ is the density in g/cm^3, m is the mass in g, and V is the volume in cm^3, M_D is the mass of the dry specimens, M_W is the mass of the wet specimens, and M_I is the mass of the immersed specimens.

Apparent composite density was determined by the Archimedes principle (Eq. (2)) following ASTM C830-00 [25], using a precision balance (0.1 mg sensitivity). Each sample was dried in an oven overnight and its dry mass, M_D, was recorded immediately after removal. Samples were then immersed in water for 3 h (to measure the M_I parameter), and the saturated mass in air, M_W, was measured afterwards.

2.2.3 Void Content

The void content was determined using two methods, an analytical method, and an experimental method. Analytically, the determination was conducted using the ASTM D2734-94 standard (Eq. (3)) [26].

$$\% \ V_V = \frac{|D_T - D_E|}{D_T} \times 100 \tag{3}$$

where % V_v is the percentage in volume of voids present in the composites, D_T is the theoretical density and D_E is the experimental density.

To determine this parameter experimentally, the Archimedes method was employed, enabling the acquisition of apparent porosity. The experimental procedure was the same used for obtaining apparent density, and Eq. (4) [26] was applied to determine the percentage of apparent porosity present in the composites.

$$\% \ P_{AP} = \frac{M_W - M_D}{M_W - M_I} \times 100 \tag{4}$$

where % P_{AP} is the percentage of apparent porosity present in the composites.

2.2.4 Mechanical Analysis

Mechanical testing was carried out using a universal testing machine (Shimadzu AG-25TA, Kyoto, Japan). Tensile tests were performed using a 20 kN load cell at a crosshead speed of 1 mm/min. Flexural properties were evaluated through a three-point bending configuration with a support span of 105 mm, using the same crosshead speed. Flexural stress and strain were calculated in accordance with the ASTM D7264 standard [23] via Eqs. (5) and (6).

$$\sigma = \frac{3PL}{2bh^2} \tag{5}$$

$$\varepsilon = \frac{6\delta h}{L^2} \tag{6}$$

The impact tests were carried out using an Avery Charpy impact testing machine (Avery, Birmingham, UK). For each condition (composite configuration and test), at least four specimens were tested, with all experiments conducted at room temperature. Fig. 2 shows examples of the test set-up for the mechanical tests performed.

2.2.5 Thermal Analysis

TGA was performed using a NETZSCH TG 209 F3 Tarsus instrument (Netzsch-Gerätebau GmbH, Wiesbaden, Germany). Samples of approximately 20–25 mg were placed in an alumina (Al_2O_3) crucible. The L400 sample was selected as a representative composite configuration for thermal analysis, as all laminates were produced using the same flax fibre reinforcement and epoxy resin matrix. Given that the only variables investigated were fibre architecture and areal weight, no significant differences in thermal degradation behaviour were expected among the composite formulations. The selected sample was analysed over a temperature range of 30°C to 600°C at a constant heating rate of 10°C·min^{-1} under a nitrogen atmosphere with a flow rate of 20 mL·min^{-1}.

DSC was carried out using a DSC 300 Select instrument (Netzsch, Selb, Germany). The experimental conditions were consistent with those used in the TGA analysis, except for the maximum temperature,

which was limited to 150°C. For this analysis, the LT sample and the epoxy resin used as the matrix material were evaluated.

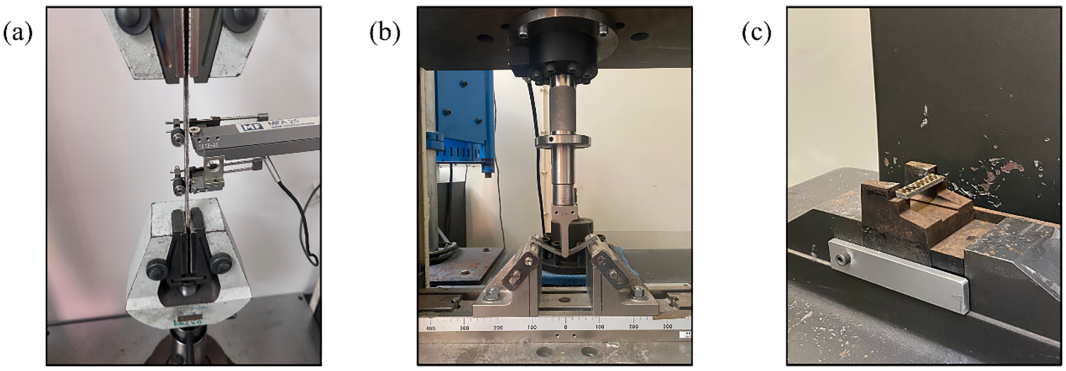

Figure 2: Example of the composite test set-up: (**a**) tensile; (**b**) flexural; (**c**) impact.

3 Results and Discussion

3.1 Morphological Analysis

Fig. 3 presents representative SEM micrographs of the different fabric architectures analysed in this study.

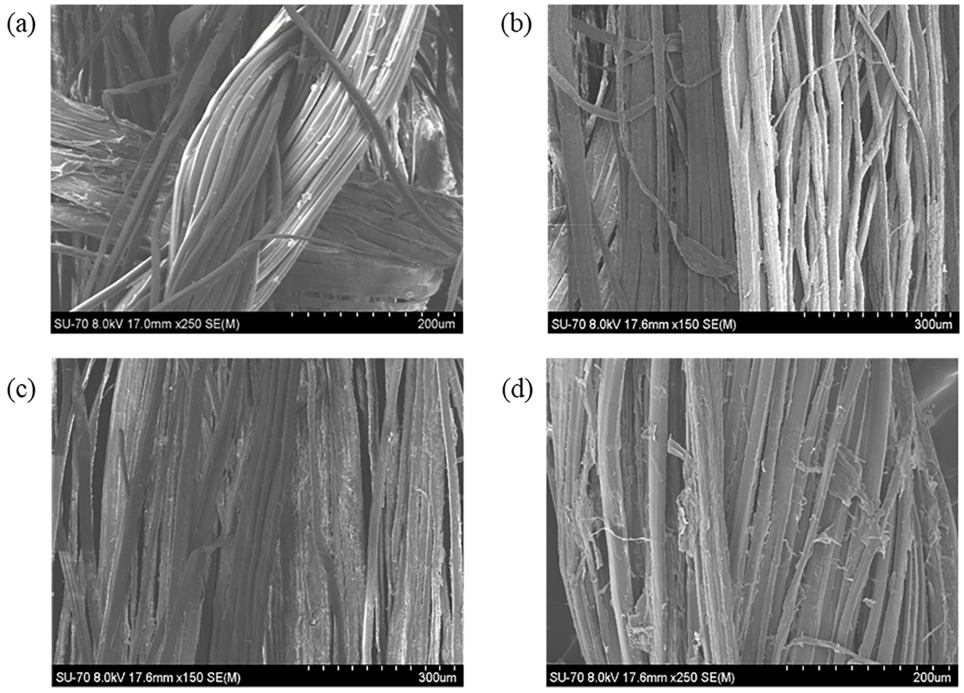

Figure 3: Representative SEM images: (**a**) Batch L250 (×250); (**b**) Batch L400 (×150); (**c**) Batch LT (×150); (**d**) Batch LB (×250).

SEM enables detailed characterisation of fibre surface topography, diameter, and inter-fibre interactions. Based on observations from Fig. 3 and consistent with findings reported in the literature [27,28], flax fibres exhibit a significantly more irregular and textured surface morphology compared to conventional synthetic

fibres. This pronounced surface roughness is a key characteristic that can strongly influence composite performance. In particular, it enhances mechanical interlocking at the fibre–matrix interface, which may improve interfacial adhesion. However, it can also promote void formation and lead to variability in wetting behaviour, ultimately affecting the overall compatibility and mechanical performance of the composite system [29].

The diameter of individual fibres was quantified using ImageJ software. For instance, for the batch L250 the diameters of the fibre were measured as 12.22 ± 5.17 μm, 13.96 ± 4.76 μm for L400, 15.70 ± 5.28 μm for LT and 14.50 ± 7.01 μm for LB. As expected, the obtained values are relatively consistent across all fabric types, reflecting the common flax fibre origin of the reinforcements. Furthermore, these results are in good agreement with values reported in the literature. For instance, Aslan et al. [30] reported average flax fibre diameters of approximately 18 μm, which is within the typical range considering the inherent variability associated with natural fibres.

3.2 Density Characterization

Table 2 presents the quantitative density measurements, demonstrating that both geometric and apparent densities remain consistent across all studied composites.

Table 2: Geometric and apparent densities of the composites studied.

Batch of Specimens	Geometric Density (g/cm^3)	Apparent Density (g/cm^3)
L250	1.16 ± 0.03	1.22 ± 0.12
L400	1.19 ± 0.02	1.27 ± 0.29
LT	1.21 ± 0.03	1.35 ± 0.20
LB	1.28 ± 0.04	1.29 ± 0.26

As the same epoxy matrix was used for all specimens, the composite densities were expected to be primarily governed by the density of the flax fibre reinforcement. This trend is confirmed by the results presented in Table 1. Furthermore, the measured values are in good agreement with those reported in the literature for flax fibre-reinforced composites. For example, Saadati et al. [31] reported a density of 1.26 g/cm^3 for unidirectional flax/epoxy composites with a fibre volume fraction of 40%, determined using the Archimedes method. This relatively low density represents a significant advantage when compared to conventional synthetic composites. For comparison, glass fibre-reinforced composites manufactured using the same epoxy resin and processing methodology exhibited a density of approximately 2.0 g/cm^3 [32]. Consequently, flax fibre composites offer considerable potential for lightweight structural applications, particularly in the automotive sector, where weight reduction directly correlates with enhanced fuel efficiency and a minimized environmental footprint.

3.3 Void Content

Table 3 shows the void content present in the different batches of composites studied.

In general, the results of apparent porosity are lower than the analytically calculated void volume results. The highest void volume was obtained for batch L250 (7.20%). This value can be explained by various factors, for instance issues during the plate processing. Inadequate bonding can lead to reduced mechanical interlocking, potentially resulting in higher porosity. Nevertheless, even the highest porosity values achieved in this work, manage to surpass some of the porosity values reported in the literature for flax fibre-reinforced composites. In a study conducted by de Kergariou et al. [10], porosity values around 20% were obtained for

flax fibre reinforced composites. A possible solution to minimize and homogenize the void content present in the batch L250 would be to apply external pressure during their processing [33]. The batches L400, LT and LB presented satisfactory results, given that, to be applied in the automotive industry, a material must exhibit a maximum of 5% porosity [34].

Table 3: Volume of voids (%) and apparent porosity (%) of the investigated composites.

Batch of Specimens	Volume of Voids (%)	Apparent Porosity (%)
L250	7.20	3.13 ± 0.20
L400	2.46	2.01 ± 0.36
LT	2.26	2.07 ± 0.36
LB	4.95	2.53 ± 0.26

3.4 Mechanical Properties

3.4.1 Tensile Properties

The representative tensile stress-strain curves are displayed in Fig. 4, while the corresponding quantitative properties, as a function of fibre architecture, are summarized in Fig. 5 and Table 4.

The tensile behaviour of the composites was strongly influenced by the fabric architecture used as reinforcement. Analysis of the experimental results indicates that composites reinforced with twill fabrics exhibited superior tensile performance, achieving strength values in the range of 85–90 MPa. These values are significantly higher than those obtained for batch LB, in which the fibres are oriented at 45° relative to the loading direction, resulting in greater deformation and reduced load-bearing capacity. This behaviour is attributed to the bidirectional nature of the twill architecture, which enables more effective load transfer and distribution along the principal fibre directions, resulting in higher tensile strength. In contrast, off-axis fibre orientations, such as in the LB configuration, promote shear-dominated deformation mechanisms, leading to lower strength but increased ductility. The tensile strength values obtained for the twill-reinforced composites are consistent with those reported by Ismail et al. [35], who observed a tensile strength of 90.43 MPa for flax/epoxy composites with a fibre weight fraction of approximately 46%.

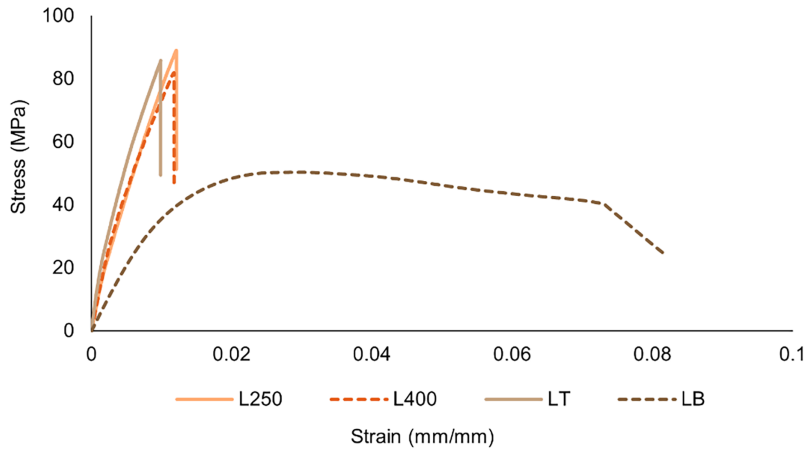

Figure 4: Representative tensile stress-strain curves as a function of reinforcement.

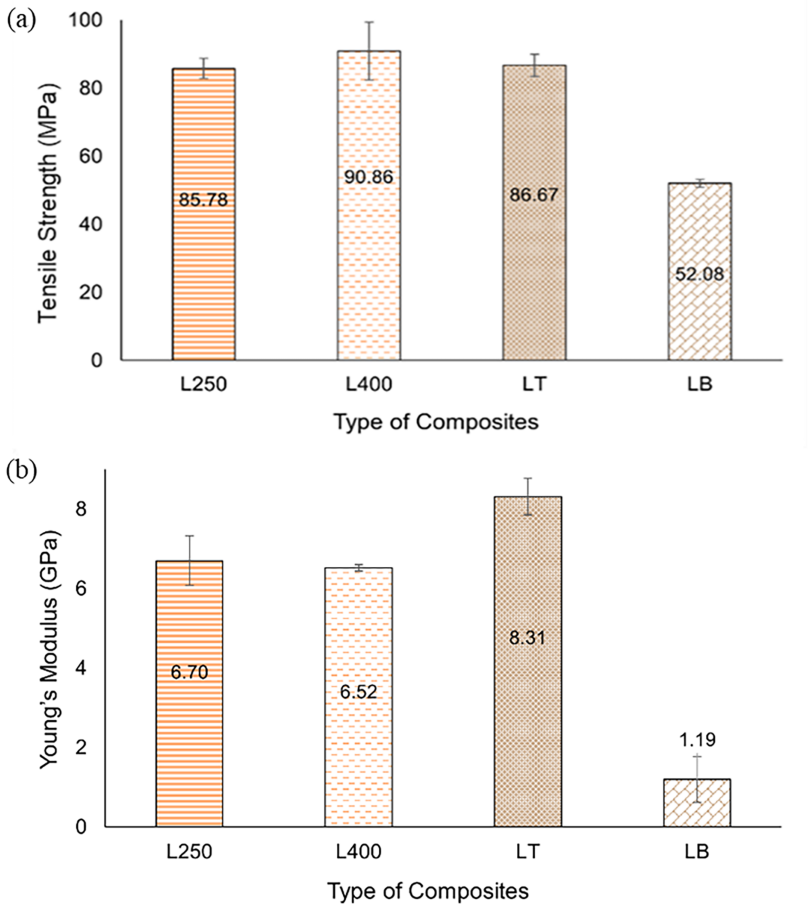

Figure 5: Tensile material properties as a function of reinforcement, (**a**) Tensile strength; (**b**) Young's modulus.

Table 4: Quantitative tensile test data as a function of fibre architecture.

Batch of Specimens	Tensile Strength (MPa)	Young's Modulus (GPa)	Strain (%)
L250	85.78 ± 2.78	6.70 ± 0.62	1.25 ± 0.06
L400	90.86 ± 8.48	6.52 ± 0.08	1.31 ± 0.13
LT	86.67 ± 3.30	8.31 ± 0.46	1.00 ± 0.09
LB	52.08 ± 1.16	1.19 ± 0.58	6.91 ± 3.04

Fabric architecture also had a significant effect on the stiffness of the composites. The highest Young's modulus was observed for the twill-reinforced composite (batch LT), reaching 8.31 GPa. This improved stiffness may be associated with its lower fibre areal weight, which can reduce the occurrence of internal defects such as voids and fibre waviness, both known to negatively affect stiffness. In contrast, the LB specimens exhibited a lower elastic modulus, consistent with their higher deformation under tensile loading, although they demonstrated comparatively greater ductility. In the LB configuration, the ±45° fibre orientation with respect to the loading direction promotes fibre rotation and in-plane shear deformation rather than direct axial load transfer through the fibres. As a result, the specimens undergo higher strain for a given applied stress, which reduces the initial slope of the stress–strain curve and leads to a lower apparent Young's modulus. The Young's modulus values obtained in this study are in good agreement with literature

data. Henschel [36] reported a modulus of approximately 8.5 GPa for bidirectional flax/epoxy composites with a twill 2/2 architecture and a fibre areal weight of 200 g/m^2, which closely aligns with the results observed for batch LT.

The fracture surfaces of different batches are presented in Figs. 6 and 7. The analysis begins with visual inspection and is followed by a detailed examination of morphological characteristics using SEM imaging. Fig. 6 shows representative tensile failures for the L400 and LB specimens, with the L250 and LT groups exhibiting similar failure patterns to L400. In Fig. 6a, the complete failure of both specimens is evident. Cracking of the resin matrix occurred on both sides, with complete debonding from the core. The core itself ruptured fully in all tested specimens. The primary difference between specimens was the fracture angle. For batches L250, L400, and LT, fabricated with twill fabrics, fractures occurred at a 90° angle relative to the tensile displacement. In contrast, batch LB exhibited fractures at a 45° angle, which is attributed to the orientation of the biaxial fibres in the composite.

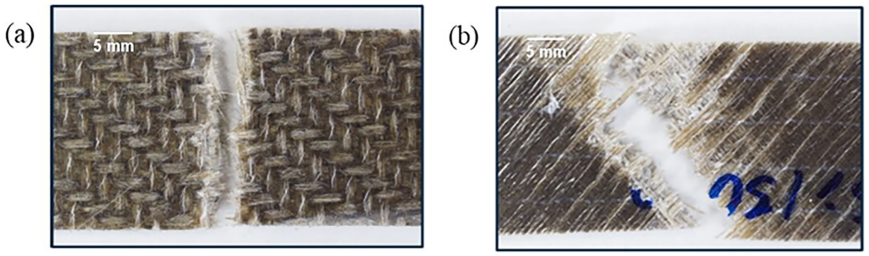

Figure 6: Representative tensile specimen failure mode: (**a**) L400; (**b**) LB.

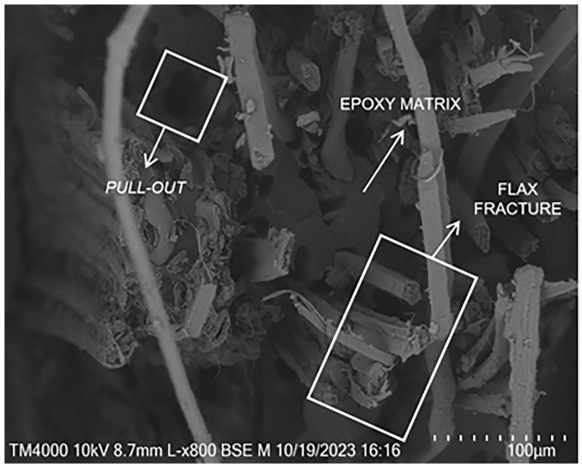

Figure 7: SEM of the fracture surface of tensile specimen: LT batch.

The microstructure in Fig. 7 reveals several important failure mechanisms. The broken flax fibres indicate they were mechanically damaged under tensile load, directly causing the material to fail. The image also shows fibres being pulled out from the epoxy matrix without breaking, which usually happens when the bond between the fibres and matrix is weak, suggesting adhesive failure at their interface. Together, fibre breakage and interfacial debonding show the complex way load is transferred, and failure happens in the sample.

3.4.2 Flexural Properties

Fig. 8 presents representative flexural stress–strain curves, while Fig. 9 and Table 5 summarize the quantitative flexural properties for each reinforcement architecture. LB specimens exhibited greater deformation before fracture, reflecting the higher ductility of the biaxial fabric compared with the twill fabrics. Consistent with fibre orientation effects observed in tensile tests, LB showed the lowest flexural strength and stiffness, while the other batches displayed similar properties. L400 was slightly superior, likely due to its higher grammage (400 g/m^2).

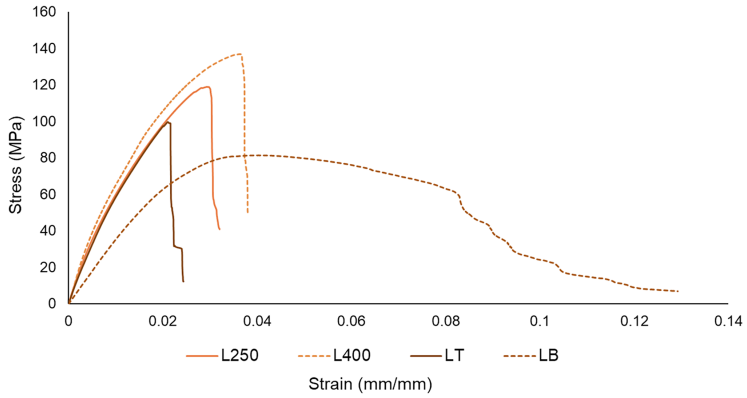

Figure 8: Representative flexural stress-strain curves as a function of reinforcement.

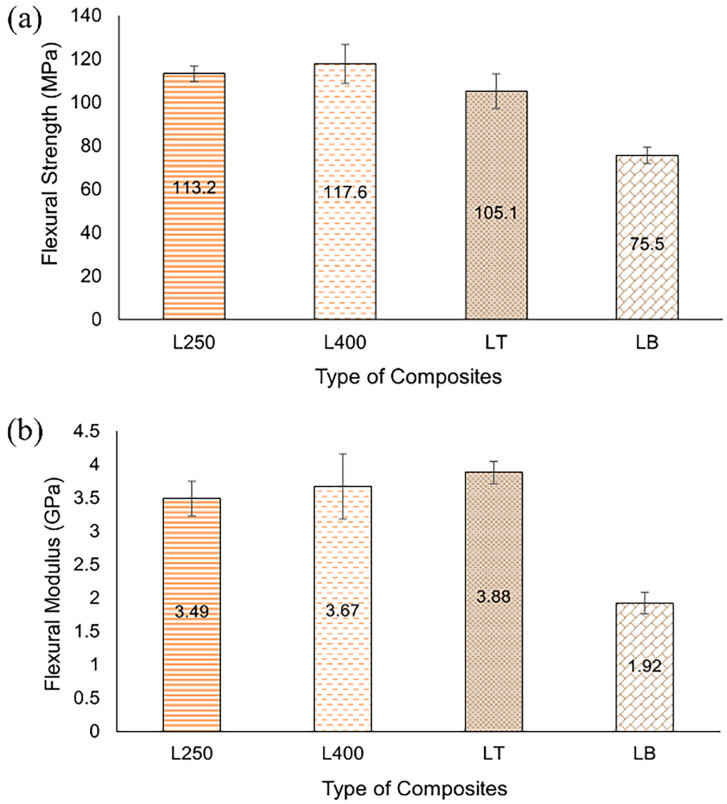

Figure 9: Flexural material properties as a function of reinforcement: (**a**) Flexural strength; (**b**) Flexural modulus.

Table 5: Quantitative flexural test data as a function of fibre architecture.

Batch of Specimens	Flexural Strength (MPa)	Flexural Modulus (GPa)	Strain (%)
L250	113.2 ± 3.6	3.49 ± 0.26	3.28 ± 0.09
L400	117.6 ± 9.0	3.67 ± 0.49	3.19 ± 0.10
LT	105.1 ± 8.0	3.88 ± 0.17	3.15 ± 0.51
LB	75.5 ± 3.7	1.92 ± 0.16	12.85 ± 1.73

As shown in Fig. 8 and Table 5, composites reinforced with twill flax fabrics exhibited superior flexural performance, with strength values ranging from 105 to 118 MPa and a flexural modulus of approximately 4 GPa. The higher flexural strength observed for the L250 and L400 batches can be attributed to their higher fibre areal weights compared to the LT specimens. Increased fibre content generally promotes more efficient load transfer within the composite, thereby enhancing resistance to failure under bending loads.

The reinforcement architecture also had a pronounced effect on flexural stiffness. In line with the tensile results, the LB batch exhibited significantly higher deformation (approximately 13%) compared to the other configurations (≈3%), resulting in a markedly lower flexural modulus. This behaviour is associated with the off-axis fibre orientation, which promotes shear-dominated deformation and reduces stiffness under bending. In contrast, the LT batch, despite its lower fibre areal weight, exhibited the highest flexural modulus. This behaviour may be attributed to improved resin impregnation and a reduced likelihood of fibre misalignment or waviness. These factors contribute to enhanced fibre–matrix interfacial bonding and more effective stress transfer, ultimately leading to improved stiffness.

Fig. 10 illustrates typical flexural failure modes for each reinforcement type. In Fig. 10a, LB specimens display a mixed failure mode, combining bottom-face tension with cross-sectional cracking, reflecting the higher compression resistance of these composites. The LT batch shows a similar pattern, with an additional region of fibre buckling under compression at the top of the specimen. Fig. 10c,d shows classic tensile failures at the specimen bottoms, with the top faces remaining largely intact.

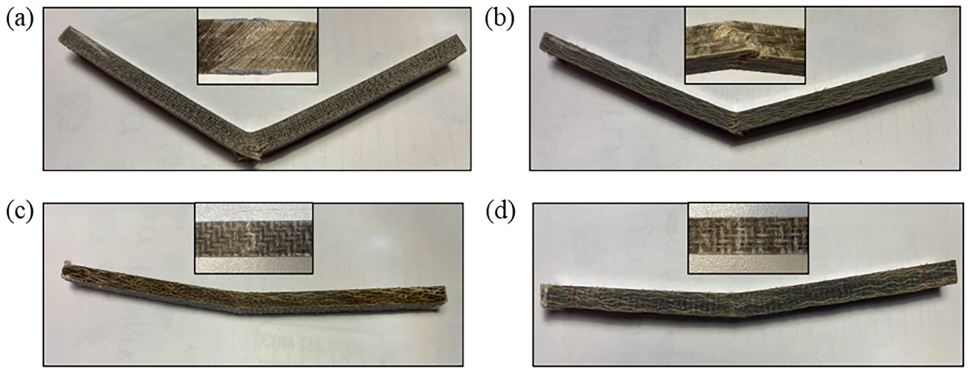

Figure 10: Representative flexural specimen failure mode as a function of reinforcement: (**a**) LB; (**b**) LT; (**c**) L400; (**d**) L250.

3.4.3 Impact Properties

Fig. 11 presents the impact energy absorption of the composites for each reinforcement type. The results show that the impact strength of the composites is strongly influenced by the choice of reinforcing fibre.

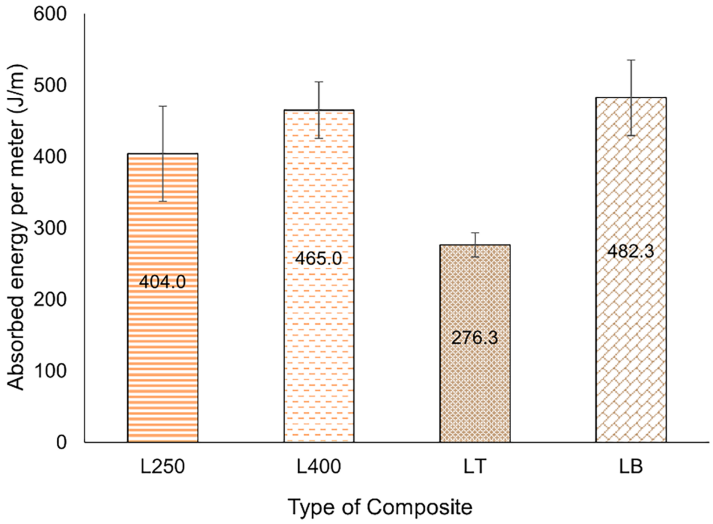

Figure 11: Impact energy absorption of the composites.

Batches L400 and LB exhibited the highest impact energy absorption, ranging from 465 to 485 J/m. The superior performance of LB, in contrast to its lower tensile and flexural properties, is attributed to its ductile behaviour, which enhances energy dissipation. Batch LT showed the lowest impact absorption, likely due to its lower fibre grammage (200 g/m^2), resulting in a reduced fibre volume fraction. This leads to a reduced fibre volume fraction, weakening stress distribution and energy dissipation while increasing brittleness. With the matrix acting as the primary load-bearing component, its lower toughness further exacerbates the composite's susceptibility to impact damage.

At the end of the Charpy tests, complete fracture was observed in all specimen batches. Local delamination was noted in some specimens of batches LT and LB. These results highlight the potential of flax-fibre-reinforced composites for automotive applications, particularly in non-structural or semi-structural components where impact absorption is critical. The high energy absorption of L400 and LB suggests suitability for interior panels (e.g., rear seat panels), knee bolsters, bumpers, and other components designed to dissipate collision energy. Nevertheless, the occurrence of total fracture indicates that improvements in fibre–matrix adhesion and overall composite toughness are needed to enhance durability and crashworthiness.

3.4.4 Thermal Properties

TGA was used to assess the thermal stability of the flax-fibre-reinforced composites across a range of temperatures. As previously discussed, one of the main limitations of natural fibre-reinforced composites is their susceptibility to thermal degradation at elevated temperatures. Since all composites were manufactured using the same type of flax fibres, batch L400 was selected as a representative sample to assess the general thermal behaviour of the developed materials. The corresponding results are presented in Fig. 12 and Table 6. Key thermal parameters, including the initial decomposition temperature (T_{IDT}), final decomposition temperature (T_{FDT}), and char residue, were determined from the TG curves. These parameters are commonly used to characterise the thermal stability of composite materials [20]. As expected, thermal degradation is associated with a significant mass loss, which is reflected by a sharp decline in the TG curve. This behaviour, highlighted by the dashed region in Fig. 12, occurs in the temperature range of approximately 300°C–400°C and corresponds to the main decomposition stage of the lignocellulosic constituents of the flax fibres.

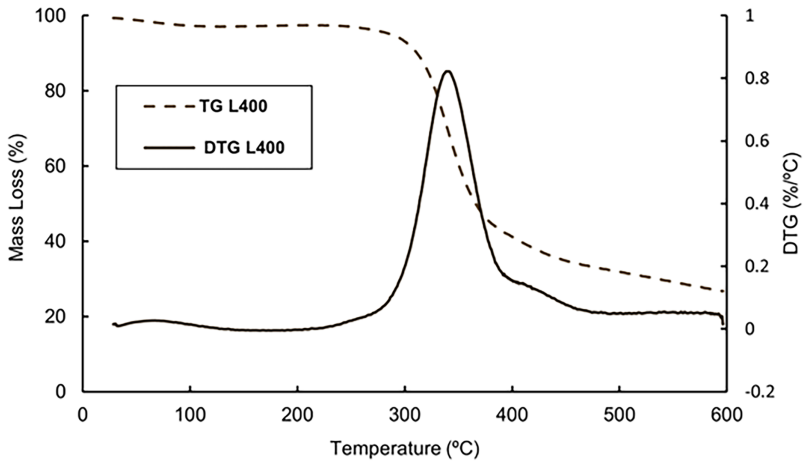

Figure 12: Representative TG and DTG curves of the batch L400.

Table 6: Thermal analysis results.

Batch of Specimens	$T_{(100°C)}$ (%)	T_{IDT} (°C)	T_{FDT} (°C)	Residual Mass (%)
L400	2.67	309.3	373.6	26.65

The derivative thermogravimetric (DTG) curve presented in Fig. 12 reveals two main degradation stages, which are characteristic of the thermal behaviour of natural fibre-reinforced composites [20]. The first stage is associated with the evaporation of absorbed moisture, occurring at relatively low temperatures. The second stage corresponds to the pyrolytic degradation of the primary lignocellulosic constituents of flax fibres, namely cellulose, hemicellulose, and lignin. This second degradation stage occurs concurrently with the thermal decomposition of the epoxy matrix, typically around 300°C [32]. The results obtained in this study are consistent with those reported by Muralidhar [37], who identified the peak degradation temperature of flax/epoxy composites in the range of 345°C–365°C.

Table 7 represents the results obtained from the DSC analysis (only the DSC results for batch LT, exemplifying the behaviour of flax-fibre reinforced composites is presented). Two predominant thermal events were observed: an endothermic peak and an exothermic peak. The endothermic peak, observed from room temperature up to approximately 86°C, is attributed to moisture evaporation (dehydration) within the composite. In contrast, the exothermic peak occurring at around 336°C is associated with the thermal degradation of cellulose and lignin components [20]. Furthermore, the measured glass transition temperature and heat capacity values are in good agreement with those reported in the literature for epoxy-based composite systems [38].

Table 7: DSC results.

Samples			
Batch LT		**Epoxy Resin**	
Endothermic Peak (°C)	**Exothermic Peak (°C)**	**T_g (°C)**	**ΔCp (J/g·K)**
85.58	336.38	81.4	0.152

4 Conclusions

This study demonstrated that both fibre architecture and areal weight play a significant role in determining the physical, mechanical, and thermal performance of flax fibre-reinforced epoxy composites manufactured by vacuum bagging. Twill 2/2 reinforced laminates exhibited superior tensile and flexural properties, with the L400 configuration achieving the highest tensile strength (90.86 MPa) and flexural strength (117.6 MPa), indicating that higher fibre areal weights enhance the load-bearing capacity of the composites. Conversely, the LT laminate, reinforced with a lower areal weight fabric, exhibited the highest Young's modulus (8.31 GPa) and flexural modulus (3.88 GPa). This suggests that the reduced fibre areal weight may enhance stiffness by promoting better fibre impregnation and reducing the concentration of defects within the composite structure. The biaxial architecture promoted greater deformation capability and energy absorption, resulting in the highest impact strength (482.3 J/m). In addition, all composites maintained low density, with the lowest value recorded for L250 (1.16 g/cm^3), highlighting their suitability for lightweight applications. Thermal analysis revealed a characteristic two-stage degradation process, with initial moisture loss occurring below approximately 86°C and the main degradation of the lignocellulosic constituents taking place around 340°C. Overall, the results demonstrate that flax fibre-reinforced epoxy composites offer a promising combination of low weight, mechanical performance, impact resistance, and thermal stability, while their properties can be effectively tailored through the selection of fibre architecture and areal weight.

Acknowledgement: Not applicable.

Funding Statement: This work was developed within the scope of the project CICECO Aveiro Institute of Materials, UID/50011/2025 (DOI 10.54499/UID/50011/2025) & LA/P/0006/2020 (DOI 10.54499/LA/P/0006/2020), financed by national funds through the FCT/MCTES (PIDDAC). Matilde Oliveira thanks Fundação para a Ciência e Tecnologia (FCT) for the PhD grant 2024.02007.BDANA.

Author Contributions: Conceptualization: Matilde Oliveira, Mariana Banea; methodology: Matilde Oliveira, Mariana Banea; formal analysis and investigation: Matilde Oliveira; writing—original draft preparation: Matilde Oliveira; writing—review and editing: Mariana Banea, Vítor Neves; supervision: Mariana Banea, Vítor Neves. All authors reviewed and approved the final version of the manuscript.

Availability of Data and Materials: Data Available upon Reasonable Request.

Ethics Approval: Not applicable.

Conflicts of Interest: The authors declare no conflicts of interest.

References

1. Skosana SJ, Khoathane C, Malwela T. Driving towards sustainability: a review of natural fiber reinforced polymer composites for eco-friendly automotive light-weighting. J Thermoplast Compos Mater. 2025;38(2):754–80. doi:10.1177/08927057241254324.
2. Dua S, Khatri H, Naveen J, Jawaid M, Jayakrishna K, Norrrahim MNF, et al. Potential of natural fiber based polymeric composites for cleaner automotive component production—a comprehensive review. J Mater Res Technol. 2023;25(6):1086–104. doi:10.1016/j.jmrt.2023.06.019.
3. Dunne R, Desai D, Sadiku R, Jayaramudu J. A review of natural fibres, their sustainability and automotive applications. J Reinf Plast Compos. 2016;35(13):1041–50. doi:10.1177/0731684416633898.
4. Nijjar S, Sudhakara P, Sharma S, Saini S. Overview on the latest trend and development on mechanical, tribological & microstructural properties of natural fibre polymer composites. Mater Today Proc. 2022;63(1):663–72. doi:10.1016/j.matpr.2022.04.733.

5. Avci A, Eker AA, Bodur MS, Candan Z. Water absorption characterization of boron compounds-reinforced PLA/flax fiber sustainable composite. Int J Biol Macromol. 2023;233:123546. doi:10.1016/j.ijbiomac.2023.123546.
6. Karimah A, Ridho MR, Munawar SS, Adi DS, Ismadi, Damayanti R. A review on natural fibers for development of eco-friendly bio-composite: characteristics, and utilizations. J Mater Res Technol. 2021;13(10):2442–58. doi:10.1016/j.jmrt.2021.06.014.
7. Jena S, Khatri VN, Nainegali L, Dutta RK. Study on physical, mechanical, morphological, and crystallographic properties of chemically treated sisal fibers. Fibres Polym. 2024;25(7):2517–34. doi:10.1007/s12221-024-00590-9.
8. Khan MAH, Ahmed A, Alaneme GU, Imtiaz M, Shabir A, Ali T, et al. Multifaceted properties and applications of natural fiber composites: from molecular dynamics to real-world uses—a comprehensive review. J Nat Fibres. 2026;23(1):2665751. doi:10.1080/15440478.2026.2665751.
9. Moudood A, Rahman A, Öchsner A, Islam M, Francucci G. Flax fiber and its composites: an overview of water and moisture absorption impact on their performance. J Reinf Plast Compos. 2019;38(7):323–39. doi:10.1177/0731684418818893.
10. de Kergariou C, Le Duigou A, Popineau V, Gager V, Kervoelen A, Perriman A, et al. Measure of porosity in flax fibres reinforced polylactic acid biocomposites. Compos Part A Appl Sci Manuf. 2021;141(12):106183. doi:10.1016/j.compositesa.2020.106183.
11. Neto J, Queiroz H, Aguiar R, Lima R, Cavalcanti D, Doina Banea M. A review of recent advances in hybrid natural fiber reinforced polymer composites. J Renew Mater. 2022;10(3):561–89. doi:10.32604/jrm.2022.017434.
12. Puttegowda M. Eco-friendly composites: exploring the potential of natural fiber reinforcement. Discover Appl Sci. 2025;7(5):401. doi:10.1007/s42452-025-06981-8.
13. Moudood A, Rahman A, Khanlou HM, Hall W, Öchsner A, Francucci G. Environmental effects on the durability and the mechanical performance of flax fiber/bio-epoxy composites. Compos Part B Eng. 2019;171:284–93. doi:10.1016/j.compositesb.2019.05.032.
14. Junior RAA, de Queiroz HFM, Banea MD. Effects of UD and twill flax reinforcements in the mechanical properties of interlaminar hybrid flax/jute composites. J Polym Res. 2025;32(12):460. doi:10.1007/s10965-025-04698-1.
15. Ahmad F, Yuvaraj N, Bajpai PK. Influence of reinforcement architecture on static and dynamic mechanical properties of flax/epoxy composites for structural applications. Compos Struct. 2021;255(1):112955. doi:10.1016/j.compstruct.2020.112955.
16. Elayaraja R, Rajamurugan G. Performance of hybrid composites fabricated by flax/hemp fibers using wire mesh plain weaving techniques. Fibres Polym. 2024;25(12):4873–83. doi:10.1007/s12221-024-00763-6.
17. Charlet K, Jernot JP, Gomina M, Bizet L, Bréard J. Mechanical properties of flax fibers and of the derived unidirectional composites. J Compos Mater. 2010;44(24):2887–96. doi:10.1177/0021998310369579.
18. Benkhelladi A, Laouici H, Bouchoucha A. Tensile and flexural properties of polymer composites reinforced by flax, jute and sisal fibres. Int J Adv Manuf Technol. 2020;108(3):895–916. doi:10.1007/s00170-020-05427-2.
19. Cerbu C. Mechanical characterization of the flax/epoxy composite material. Procedia Technol. 2015;19(1):268–75. doi:10.1016/j.protcy.2015.02.039.
20. Neto JSS, de Queiroz HFM, Aguiar RAA, Banea MD. A review on the thermal characterisation of natural and hybrid fiber composites. Polymers. 2021;13(24):4425. doi:10.3390/polym13244425.
21. Dong Z, Ding RY, Zheng L, Zhang X, Yu CW. Thermal properties of flax fiber scoured by different methods. Therm Sci. 2015;19(3):939–45. doi:10.2298/tsci130329005z.
22. ASTM D3039/D3039M-14. Standard test method for tensile properties of polymer matrix composite materials. West Conshohocken, PA, USA: ASTM International; 2014.
23. ASTM D7264/D7264M-15. Standard test method for flexural properties of polymer matrix composite materials. West Conshohocken, PA, USA: ASTM International; 2015.
24. ASTM D4812-11. Standard test method for unnotched cantilever beam impact resistance of plastics. West Conshohocken, PA, USA: ASTM International; 2011.
25. ASTM C830-00. Standard test methods for apparent porosity, liquid absorption, apparent specific gravity, and bulk density of refractory shapes by vacuum pressure. West Conshohocken, PA, USA: ASTM International; 2023.

26. ASTM D2734-94. Standard test methods for void content of reinforced plastics. West Conshohocken, PA, USA: ASTM International; 1994.
27. Brugaletta F, Becher AF, Rostagno DL, Kim J, Fresneda Medina JI, Ziejewska C, et al. The different properties of geopolymer composites reinforced with flax fibers and carbon fibers. Materials. 2024;17(11):2633. doi:10.3390/ma17112633.
28. Queiroz H, Pastor V, Neto J, Cavalcanti D, Banea MD. Mechanical characterization of jute/carbon hybrid epoxy composites. Proc Inst Mech Eng Part L J Mater Des Appl. 2025;239(9):1719–29. doi:10.1177/14644207241233947.
29. Liang S, Gning PB, Guillaumat L. Quasi-static behaviour and damage assessment of flax/epoxy composites. Mater Des. 2015;67(5):344–53. doi:10.1016/j.matdes.2014.11.048.
30. Aslan M, Chinga-Carrasco G, Sørensen BF, Madsen B. Strength variability of single flax fibres. J Mater Sci. 2011;46(19):6344–54. doi:10.1007/s10853-011-5581-x.
31. Saadati Y, Lebrun G, Chatelain JF, Beauchamp Y. Experimental investigation of failure mechanisms and evaluation of physical/mechanical properties of unidirectional flax-epoxy composites. J Compos Mater. 2020;54(20):2781–801. doi:10.1177/0021998320902243.
32. Oliveira M, Neves V, Banea MD. Mechanical and thermal characterization of bamboo and interlaminar hybrid bamboo/synthetic fibre-reinforced epoxy composites. Materials. 2024;17(8):1777. doi:10.3390/ma17081777.
33. Yalcinkaya MA, Sozer EM, Altan MC. Effect of external pressure and resin flushing on reduction of process-induced voids and enhancement of laminate quality in heated-VARTM. Compos Part A Appl Sci Manuf. 2019;121:353–64. doi:10.1016/j.compositesa.2019.03.040.
34. Mehdikhani M, Gorbatikh L, Verpoest I, Lomov SV. Voids in fiber-reinforced polymer composites: a review on their formation, characteristics, and effects on mechanical performance. J Compos Mater. 2019;53(12):1579–669.
35. Ismail AS, Jawaid M, Zainudin ES, Yahaya R, Alothman OY, Abu-Jdayil B, et al. Dimensional stability, mechanical and thermal performance of flax/carbon/kevlar reinforced bio-phenolic/epoxy hybrid composites. J Nat Fibres. 2025;22(1):2461491. doi:10.1080/15440478.2025.2461491.
36. Henschel K. Biocomposites in helicopter structures on the example of flax and its hybrids [master's thesis]. Munich, Germany: Technical University of Munich; 2019.
37. Muralidhar BA. Study of flax hybrid preforms reinforced epoxy composites. Mater Des. 2013;52:835–40. doi:10.1016/j.matdes.2013.06.020.
38. Griffin D, Wood S, Hamerton I. Measurement of the glass transition temperature of an epoxy resin using principal components of Raman spectra. Compos Part B Eng. 2020;200:108210. doi:10.1016/j.compositesb.2020.108210.